# Automated system for maintaining a set engine speed

Mykola Yeremiyev[1,*,†], Dmytro Krytskyi[1,†], Oleksii Popov[1,†], Andry Bykov[1,†], Sergiy Karatanov[1,†] and Elvira Kaidan[1,†]

[1]*National Aerospace University H.E. Zhukovsky "Kharkiv Aviation Institute", Vadym Manko Str., 17, Kharkiv, 61070, Ukraine*

**Abstract**

The subject of the study is the process of creating an automated system for maintaining stable UAV motor speed by adaptively adjusting the angle of variable-pitch propeller blades. The aim is to develop a high-precision control system capable of autonomous operation in real time. Objectives: to analyze the technical factors of flight destabilization during the transition between helicopter and airplane schemes; to analytically determine the actual engine speed using the GFC; to create a model of the video processing and automated control system suitable for autonomous operation; to test the model in a simulation environment. The methods used are system analysis, artificial intelligence methods for detecting and recognizing markers in a video stream, system programming approaches for implementing automatic control algorithms, and a simulation modeling method for verifying solutions. The following results were obtained: the parameters of the PID controller were selected (kp=3.7; ki=0.017; kd=15), the program for Arduino was implemented, the video processing subsystem was created, the experimental stand was designed, and the effectiveness of stabilizing the speed of the internal combustion engine with a HGV was confirmed. Conclusions: The testing of the developed system showed high accuracy and stability in typical scenarios. The results can be the basis for further research on multicopters with internal combustion engines.

**Keywords**

controller, multicopter, Arduino controller, preservation of engine speed, variable pitch screw

## 1. Introduction

As the name suggests, UAVs are aircraft and require takeoff and landing sites [1]. The requirements for the size and technical equipment of the sites are determined by the type of UAV used. All UAVs can be divided into two main classes: UAVs with propellers and UAVs with bearing aerodynamic surfaces. For UAVs of the first type, the size of the platforms required for takeoff and landing is small and comparable to the size of the UAV itself. To ensure the takeoff and landing of the second type of UAV, even with the use of additional equipment (catapult for takeoff and parachute for landing), the size of the sites must be much larger, and significant restrictions are imposed on the size and location of the buildings surrounding such sites, unlike the first type. At the same time, UAVs with load-bearing aerodynamic surfaces have a much longer flight range and barrage time than UAVs with propellers with equal energy capabilities [2].

An attempt to combine the advantages of both multi-rotor and fixed-wing unmanned aerial vehicles (UAVs) is the use of convertible airplanes. However, the creation of such vehicles is accompanied by a number of technical difficulties. One of the main problems is to ensure sufficient stability and control during takeoff and landing modes, when the convertible airframe operates in a vertical mode and is a statically unstable aircraft. This problem can be partially solved by using electric motors as a lifting power plant. Due to their good dynamic characteristics, electric motors provide precise control of the rotor speed over a wide range of loads, which allows the use of constant pitch propellers. This approach reduces the complexity of the control system and increases the reliability of the vehicle in vertical

**Figure 1:** Test bench for modeling the ICE+GOK system.

flight modes [3]. However, in horizontal flight mode, the use of electric motors and batteries creates additional mass costs, which leads to a decrease in the payload of the vehicle. The energy intensity of modern batteries also remains a limiting factor, which limits the duration and range of flight [4]. Although the use of electric motors as propulsion is also possible, the effectiveness of such a solution directly depends on the improvement of energy storage elements. One of the most promising areas is the hybridization of energy systems, where electric motors are used only in vertical modes, and the flight is carried out by internal combustion engines [5].

In order to ensure the stability of the aircraft during transitions between flight modes, even in the case of partial drive failures, modern research in the field of controlling convertible aircraft proposes the use of adaptive algorithms [6].

The solution to the problem would be the use of internal combustion engines (ICEs) for both propulsion and lifting motors, since at the moment the energy capacity to weight ratio of a battery is significantly inferior to liquid organic fuel. The most advantageous would be the use of multi-rotor schemes for take off and landing, but since the dynamic characteristics of an internal combustion motor are much worse than those of an electric motor, the task of ensuring the stability of aircraft in take off and landing modes is significantly complicated. It is possible to improve the dynamic characteristics of the "ICE + main rotor" system by using a variable pitch screw (VPS). In this case, the ICE can operate at a given constant speed, and the value of the lifting force can be changed due to the angle of the blades (pitch) of the propeller. As noted above, the ICE is significantly inferior to the electric motor in its dynamic characteristics, which required the development of a system to stabilize the rotational speed of the ICE shaft when the external load changes.

A similar system was modeled using an electric motor and a GOK. The stability of the rotor speed was ensured by a controller built on a microprocessor-based system. The simulation was performed with different types of controllers, and it showed the possibility of ensuring the constancy of the rotational speed of the electrode motor when the pitch of the screw changes. This made it possible to proceed to the next stage - the creation of a test bench for the ICE+GOK system shown in Figure 1. As noted above, the ICE is significantly inferior to the electric motor in terms of its dynamic characteristics, which required the development of a system to stabilize the rotational speed of the ICE shaft in the
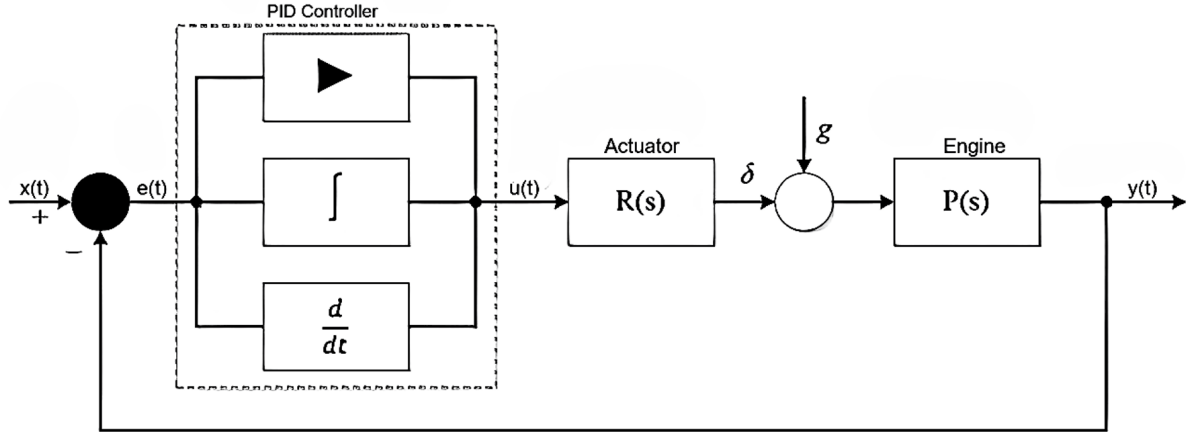
**Figure 2:** Block diagram of a system with a PID controller.

event of a change in external load.

Unmanned aerial vehicles (UAVs) have recently become one of the fastest growing types of aviation. UAVs are widely used in various spheres of life [7]. However, despite significant progress in the development of UAVs in recent years, there are still a number of problems with their practical use. These are primarily legal, technical and energy problems. The development of small unmanned aerial vehicles (UAVs) that implement the convertible airframe scheme is accompanied by a number of technical difficulties. In particular, one of the main problems is the delay in the response of the internal combustion engine (ICE) to control signals, which makes it difficult to ensure the stabilization of the vehicle.

Another critical task is to ensure a stable lift during the transition between helicopter flight and airplane flight modes. One of the technically feasible solutions to this problem is the introduction of a variable pitch propeller. This approach makes it possible to adjust the lift force without changing the engine speed, only by changing the angle of attack of the rotor blades. This, in turn, requires maintaining a constant engine speed, which is possible only if a proportional-integral-differential regulator (PID) or a three-position controller is used [8].

Despite the remarkable progress in the field of automatic control theory achieved by scientists around the world in recent years, PID controllers are still the most common in industrial applications. Their popularity is due to a number of important advantages: they have a simple design, can be easily implemented in various systems, demonstrate a clear and stable operating principle, effectively cope with most practical tasks, and require relatively low implementation costs. It is the combination of availability, reliability, and versatility that makes PID controllers a key tool in the automation of technical processes .

For the system to be sustainable, it is necessary to $\Re\left(p_{1,2}\right) < 0$, when $\xi > 0$. Moreover, if $\xi < 1$, then we obtain a damped oscillatory transient, and if $\xi > 1$ the transient will be aperiodic.

## 1.1. Realization of the PID controller

PID controllers, also known as three-component controllers, play an important role in feedback automatic control systems. They are widely used in industry and in tasks that require continuous and precise control. Thanks to their ability to provide stable operation under conditions of changing parameters and loads, PID controllers have become an indispensable tool in many areas of technology. The controller continuously calculates the error $e(t)$ - the difference between the desired value of the input signal and the actual result of the system - and generates a control influence based on three components: proportional (P), integral (I), and differential (D). It is thanks to these components that it got its name [9, 10].

A block diagram of the system with a PID controller is shown in the Figure 2.
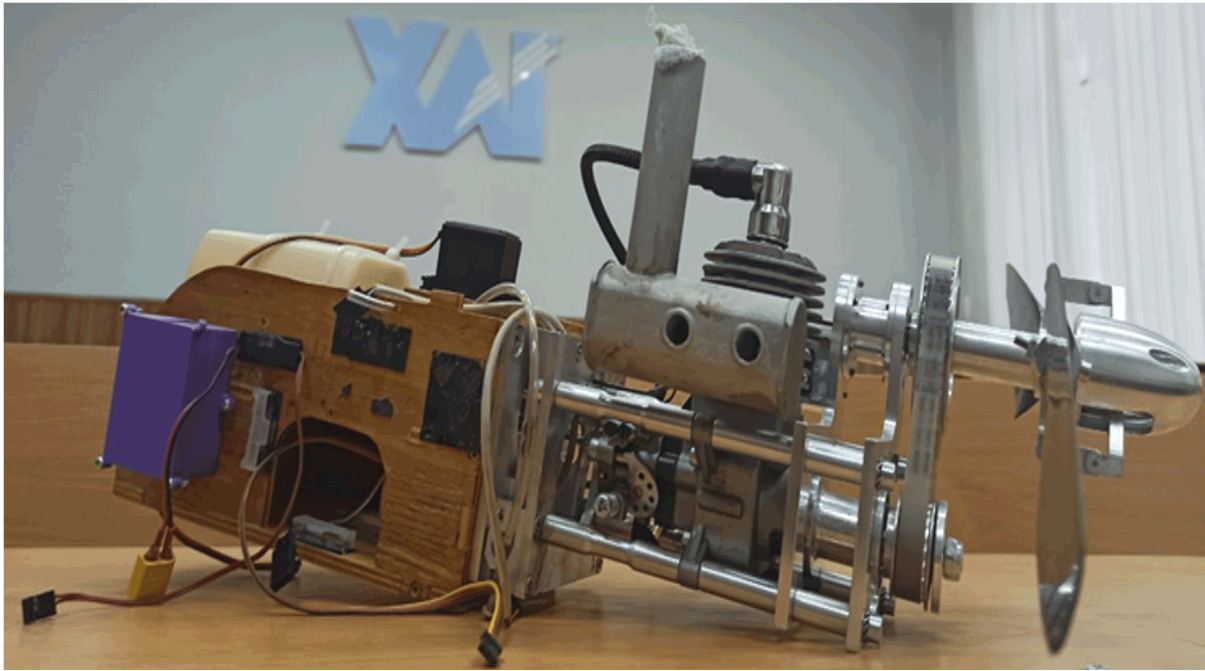
**Figure 3:** Motor with shaft speed stabilization.

The diagram under consideration contains a number of key notations that illustrate the operation of an automatic control system with a PID controller:

- $x(t)$ is the setpoint signal, in this case, the desired speed received by the receiving device;
- $y(t)$ is the actual speed value that the system provides in real time;
- $e(t)$ is the error or deviation, defined as the difference between the setpoint signal $x(t)$ and the measured value $y(t)$;
- $u(t)$ is control action generated by the PID controller based on the error analysis;
- $\delta$ is the signal processed by the actuator (drive), interpreted as a transformation of the control action;
- $g$ - an external disturbance, for example, caused by a change in the angle of attack of the propeller blades;
- Adder is a device that performs mathematical addition of signals. The shaded lower part of the symbol indicates that one of the signals (feedback) has a negative value, i.e., is subtracted;;
- Block marked "▶" is the designation of the proportional link that calculates the product of the error $e(t)$ and the corresponding gain;
- Integral block is the integration link that accumulates the error value over time and scales it by the corresponding coefficient, smoothing out short-term deviations.
- Block with the designation $\frac{d}{dt}$ is differentiator – multiplies the difference of the given output signal with the output signal at the previous moment.

## 2. The control system of the ICE+GOK

### 2.1. System for stabilizing the rotational speed of an ICE with GOK

The functional diagram of an internal combustion engine with shaft speed stabilization is shown in Figure 3 and includes the engine We and the regulator $Wr$ [10]. The input parameter is the set motor shaft speed $\omega*$, and the output parameter is the actual shaft speed $\omega$. The motor shaft is loaded with a GOK, the moment of resistance of which is determined by the angle of the propeller blades $\theta$.

Changing the angle $\theta$ creates a disturbing effect that is compensated by the $Wr$ controller. The $Wr$ input is fed with a mismatch signal $\varepsilon = \omega^* - \omega$, and the output is a signal to control the carburetor throttle angle $\varphi$. The operation of the motor is generally described by the equation:

$$J\frac{d\omega}{dt} = M_\varphi\left(\omega, \varphi\right) \tag{1}$$

where $J$ is the total moment of inertia reduced to the motor shaft, $M_\varphi$ is the motor shaft torque, and $M_\varphi$ is the shaft load resistance moment.

The motor operation mode is (equilibrium) if the values of its operating parameters do not change over time. We represent the values of the parameters in the form:

$$X = X_0 + X' \tag{2}$$

where $X$ is the actual value, $X_0$ is the value corresponding to the balance mode, and $X'$ is the disturbance.

For the case of small disturbances, the motor characteristics $M_\varphi$ and its load $M_\theta$ can be replaced by their linear approximations:

$$M_\varphi = M_{\varphi 0} + \left(\frac{\partial M_\varphi}{\partial \omega}\right)_0 \omega' + \left(\frac{\partial M_\varphi}{\partial \omega}\right)_0 \varphi'.$$

$$M_\theta = M_{\theta 0} + \left(\frac{\partial M_\theta}{\partial \omega}\right)_0 \omega' + \left(\frac{\partial M_\theta}{\partial \omega}\right)_0 \theta'. \tag{3}$$

Since for the steady-state regime $\omega = \omega_0$ and $M_{\varphi 0} = M_{\theta 0}$, after substituting (3) into (1), we obtain the linearized equation for perturbations

$$J\frac{d\omega}{dt} + \left[\left(\frac{\partial M_\theta}{\partial \omega}\right)_0 - \left(\frac{\partial M_\varphi}{\partial \omega}\right)_0\right] \cdot \omega' = \left(\frac{\partial M_\varphi}{\partial \varphi}\right)_0 \cdot \varphi' - \left(\frac{\partial M_\theta}{\partial \omega}\right)_0 \cdot \theta'. \tag{4}$$

The stability of the equilibrium mode of the motor is determined by the imbalance of the shaft torque and the load resistance torque and is evaluated by the stability factor $F_s$ [2]:

$$F_s = \frac{\Delta M}{\Delta \omega} = \frac{M_\theta - M_\varphi}{\omega'} = \left(\frac{\partial M_\theta}{\partial \omega}\right)_0 - \left(\frac{\partial M_\varphi}{\partial \omega}\right)_0. \tag{5}$$

If $F_s > 0$, the mode of operation is stable, otherwise it is unstable. Let us rewrite equation (4) in a more convenient form for analysis:

$$T_e\frac{d\omega'}{dt} + k_e\omega' = \varphi' + k_l\theta' \tag{6}$$

where $\xi_\varphi = \left(\frac{\partial M_\varphi}{\partial \varphi}\right)_0$ is steepness of the motor load characteristic; $\xi_e = -\left(\frac{\partial M_\theta}{\partial \theta}\right)_0$ is steepness of the screw load characteristic; $T_e = \frac{J}{\xi_\varphi}$ is motor time constant; $k_e = \frac{F_S}{\xi_\varphi}$ is self-leveling coefficient; $k_l = \frac{\xi_\theta}{\xi_\varphi}$ is load amplification factor.

Let the functions $\omega'_\varphi$ and $\omega'_\theta$ be the solutions of equations:

$$T_e\frac{d\omega'}{dt} + k_e\omega' \ , T_e d\omega\theta' dt + k_e\omega\theta' = k_l\theta'. \tag{7}$$

Then the solution of equation (6) is given as the sum of the solutions of equations (7):

$$\omega' = \omega'_\varphi + \omega'_\theta. \tag{8}$$

According to (7), the transfer function of the motor $W'_e$ in terms of $\varphi'$ is:

$$W'_e\left(p\right) = \frac{1}{T_e \cdot p + k_e} \tag{9}$$

and the transfer function in terms of $\theta'$ can be represented as $(k_l \cdot W_e')$, the engine can be considered as a first-order aperiodic link. Let's write the transfer function of the system for the perturbation of the angle of inclination of the propeller blades $\theta'$:

$$W_\theta' = \frac{k_l \cdot W_e'}{1 + W_r \cdot W_e'}. \tag{10}$$

The block diagram of the motor shaft speed stabilization system, constructed according to equations (7, 8), is shown in Figure 3. If the controller $W_r$ is a proportional link with a transmission coefficient $k_r$ (i.e., $W_r = k_r$), the transfer function of the system $W\theta'$ (10) will take the form:

$$W_\theta'(p) = \frac{1}{T_e \cdot p + k_e + k_r}. \tag{11}$$

In order for a system to be sustainable, the following conditions must be true $k_e + k_r > 0$.

In this case, the response $\omega'$ to a perturbation of the propeller blade angle $\theta'$ will be a monotonically decreasing function. To evaluate the sensitivity of the system and the duration of transients, we will reduce $W_\theta'$ to the standard form:

$$W_\theta'(p) = \frac{k}{T \cdot p + 1} \tag{12}$$

where $T = \frac{T_e}{k_e + k_r}$ is time constant of a closed system; $k = \frac{k_l}{k_e + k_r}$ is gain of the closed load system.

Therefore, by increasing the transmission coefficient $kr$, it is possible to reduce the sensitivity of the system to disturbances $\theta'$ and reduce the transient time constant.

With a proportional-integral controller with a transfer function $W_r(p) = k_r + \frac{1}{T_i \cdot p}$ for the transfer function of the system $W_\theta$ (10), we obtain:

$$W_\theta'(p) = \frac{k \cdot T_i \cdot p}{T_e \cdot T_i \cdot p^2 + (k_e + k_r) \cdot T_i \cdot p + 1} \tag{13}$$

or in the standard form:

$$W_\theta'(p) = \frac{k \cdot T \cdot p}{T^2 \cdot p^2 + 2\xi T \cdot p + 1} \tag{14}$$

where $T = \sqrt{T_e \cdot T_i}$ is time constant of a closed system; $\xi = \frac{k_e + k_r}{2} \cdot \sqrt{\frac{T_i}{T_e}}$ is attenuation coefficient; $k = k_l \cdot \sqrt{\frac{T_i}{T_e}}$ gain of the closed load system.

The function $W\theta$ has two poles.

When calibrating the thermistor head M5-43 at each of the control frequencies, its efficiency is determined $K_e$ according to the relation (1) or in the standard form:

$$p_{1,2} = -T \cdot \left( \xi \pm \sqrt{\xi^2 - 1} \right) \tag{15}$$

For the system to be sustainable, it is necessary that $\mathcal{R}(p_{1,2}) < 0$, which, obviously, is fulfilled when $\xi > 0$. Moreover, if $\xi < 1$, then we obtain a damped oscillatory transient, and when $\xi > 1$, the transient will be aperiodic. The introduction of a differential component, i.e., the transition to a proportional-integral-differential (PID) controller, makes it possible to improve the transient.

## 2.2. Digital realization of the PID controller

With the transition to digital control systems, the classical PID controller has gained a new life in electronic form. The digital implementation of this algorithm allows for precise and flexible control of technical processes based on feedback [11]. This approach is based on the analysis of the difference between the desired signal value and the actual system output $(e(t))$, which is processed through a mathematical combination of three components - proportional, integral, and differential. Unlike analog circuits, the digital version of the PID controller is easily programmable, scalable to the needs

of the system, and can operate in real time on the basis of microcontrollers or FPGAs. This makes it particularly attractive for modern industries that require precise, adaptive, and stable control - from drones and robots to complex industrial plants [9, 11].

In the presented structure of the digital PID controller, the differential component works separately with the feedback signal coming from the object. This signal is compared with the setpoint value - the result is the control error, which is calculated as their difference [12, 13].

After determining this error, it is fed to two channels in parallel: proportional and integrating. The proportional part reacts instantly to the deviation value, while the integral part accumulates the error value over time to eliminate systematic shifts [14]. The output signals of both channels are summed up to form a single control influence that is sent to the control system to achieve stable operation [15].

Numerical calculations, it is advisable to use normalized dimensionless quantities instead of dimensional parameters to give generality to the results, reduce the influence of the finite bit depth of the computer on the calculation results, and reduce rounding errors [16] In the digital implementation of the PID controller, it is more convenient to take into account the proportional component when normalizing the input digitized signal. Therefore, the transfer function of the PID controller is written without the proportional component:

$$W_{R(p)} = \left(1 + \frac{1}{T_i \cdot p}\right) \cdot (1 + T_i \cdot p) = \frac{T_i T_d \cdot p^2 + (T_i T_d) \cdot p + 1}{T_i + p}. \tag{16}$$

This transfer function corresponds to the differential equation

$$T_i T_d \cdot x' + (T_i T_d) \cdot x' + x = T_i \cdot y' \tag{17}$$

here $x$ is the input signal, $y$ is the output signal. To integrate equation (17), we use the difference method, the essence of which is to exclude the limit transition during differentiation. In this case, the values of the derivatives of the function are replaced by the difference of its values taken with a fixed interval $\Delta t$.

Depending on the method of approximating the derivatives, there are many varieties of ordinary difference methods. Let $q_i$ be the values of a certain function taken in steps $\Delta t = \tau$. To approximate the first derivative, consider the expansion of the function $q(t)$ into a static series in the neighborhood of the point $t = t_i$:

$$q(t) = q(t_i) + \sum_{n=1}^{\infty} \frac{q^{(n)}(t_i) \cdot (t - t_i)^n}{n!} \tag{18}$$

For points $t_i$ and $t_i - 1 = t_i - \tau$ we will get

$$q(t_i) = q_i q(t_{i-1}) = q(t_i - \tau) = q_{i-1} - q_i' \cdot \tau + q_i'' \cdot \frac{\tau^2}{2!} - \ldots, \tag{19}$$

from where we express $q'i$:

$$q_i' = \frac{q_i - q_{i-1}}{\tau} + \frac{q_i'' \cdot \tau}{2!} + \ldots = \frac{q_i - q_{i-1}}{\tau} + O(\tau). \tag{20}$$

The resulting expression approximates $q'i$ with an error proportional to the step $\tau$, i.e., with the first order of approximation. Similarly, we can obtain an approximation of the derivatives with a large order of approximation. In particular, the formulas for the first and second derivatives with the first order of approximation are as follows:

$$q_i' = \frac{q_i - q_{i-1}}{\tau} + O(\tau) \, ; q_i' = \frac{q_i - 2q_{i-1} + q_{i-2}}{\tau^2} + O(\tau) \tag{21}$$

and with the second order of approximation (the error is proportional to $\tau 2$)

$$q_i' = \frac{3q_i - 4q_{i-1} + q_{i-2}}{2\tau} + O(\tau^2) \, ; q_i' = \frac{2q_i - 5q_{i-1} + 4q_{i-2} - q_{i-3}}{\tau^2} + O(\tau^2) \tag{22}$$
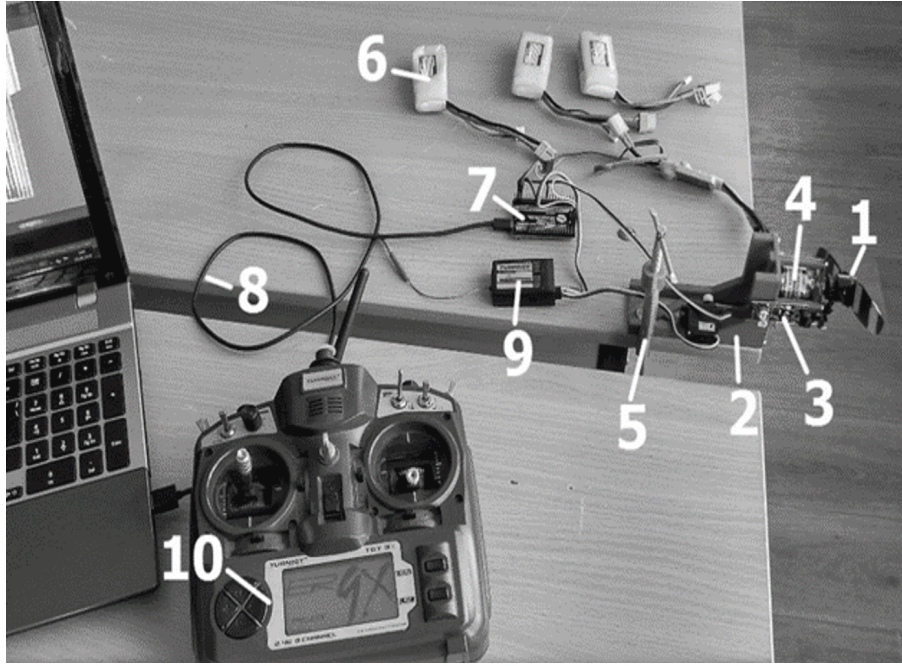
**Figure 4:** The test bench ready for operation: 1 - GOK, 2 - 3D printed model, 3 - distance sensor, 4 - motor, 5 - clamp, 6 - battery, 7 - Arduino controller, 8 - USB cable, 9 - receiver, 10 – transmitter.

Formulas (21) and (22) are called one-sided difference estimators because they express the derivatives through the values of the function at the current and several previous moments. By denoting

$$\Delta q_i = q_i - q_{i-1}, \Delta^2 q_i = \Delta q_i - \Delta q_{i-1} = q_i - 2q_{i-1} + q_{i-2} \tag{23}$$

rewrite (21, 22) in the form:

$$q_i' = \frac{1}{\tau}\Delta q_i + O(\tau), q_i'' = \frac{1}{\tau^2}\Delta^2 q_i + O(\tau), q_i' = \frac{1}{\tau}\Delta q_i + 0.5\Delta^2 q_i + O(\tau^2),$$

$$q_i'' = \frac{1}{\tau^2}2(\Delta^2 q_i + \Delta^2 q_{i-1}) + O(\tau^2). \tag{24}$$

Let us write the controller equation (17) for time $t = t_i$, substituting their second-order approximations instead of derivatives (23, 24):

$$\frac{T_i T_d}{\tau^2} \cdot (2\Delta^2 x_i - \Delta^2 x_i - 1) + \frac{T_i T_d}{\tau^2} \cdot (\Delta x_i - 0.5\Delta^2 x_i) + x_i = \frac{T_i}{\tau} \cdot (\Delta y_i + 0.5\Delta^2 y_i). \tag{25}$$

Let's bring the constant times of the controller to the period $T_1 = T_i/\tau, T_2 = T_d/\tau$ and solve (25) with respect to $\Delta y_i$, from which we find $y_i$:

$$\Delta y_i = \left(\frac{1}{3}\Delta_{i-1} + \frac{3}{2} \cdot \frac{1}{T_1} \cdot x_i\right) + \left(1 + \frac{T_2}{T_1}\right) \cdot \left(\Delta x_i - \frac{1}{3}\Delta x_{i-1}\right) + \frac{2}{3} \cdot T_2 \cdot (2\Delta^2 x_i - \Delta^2 x_i - 1), \tag{26}$$

$$y_i = y_{i-1} + \Delta y_i.$$

## 3. Creation of an automated system for controlling the speed of a variable pitch screw

An important step in creating an automated system is to build a mockup for developing and testing the regulator (Figure 4). The non-contact infrared sensor YL-63 (FC-51) detects objects in the distance range from almost 0 to the set limit without coming into direct contact with them. This sensor is intended

**Figure 5:** Variable pitch screw.

for use when information about the distance to an object is not required, but only about its presence or absence [17, 18]. The detection distance depends on the settings, which can be changed using the built-in potentiometer. The device works by determining the illumination of the photodetector. Since the YL-63 records reflected radiation, there is a distance measurement error caused by the different reflectivity of the surfaces of objects made of different materials. The sensor used operates in a discrete mode and responds to changes in the intensity of infrared (IR) radiation returned by objects in the monitored area. These changes are usually caused by the movement of surrounding objects or moving parts of structures.

The device contains an infrared signal emitter and a photosensitive element - a photodetector. The IR light reflected from the obstacle hits the photodetector, which transmits the signal to the LM393 comparator. The latter is configured to react when a certain level of illumination is reached, outputting a logical "1" or "0" signal.The YL-63 sensor is a diffusion type, which means that its principle of operation is based on the ability of light to scatter in different directions after being reflected from a surface. It is this diffusion that provides detection of the presence of an object.

The function of the device is to record the level of light reaching the photodetector. However, since the sensor responds to reflected light, the detection accuracy may vary depending on the material and color of the object's surface. Surfaces with different reflection coefficients cause measurement errors.

The assembled variable pitch screw is shown in Figure 5. The diagram of connecting the elements to the board is shown in Figure 6.

The result of assembling the layout with the designation of the components is shown in Figure 2. During the testing phase, the YL-63 sensor model demonstrated unstable operation. The main problem was its excessive sensitivity to external light interference: when additional light sources appeared, the device generated false signals. In this regard, it was decided to replace the YL-63 with a more reliable model - KY-032. The KY-032 sensor allows you to detect objects without the need for physical contact with them, which ensures the fixation of the presence of obstacles at a certain distance. Although the device does not provide an accurate distance measurement, it reliably signals the presence of an
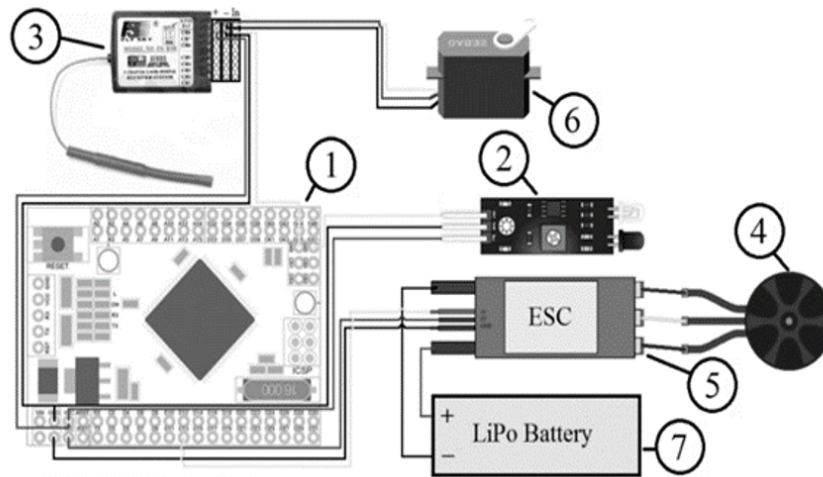
**Figure 6:** Diagram of connection of elements to the Arduino controller: 1 - Arduino Mega 2560 controller, 2 - distance sensor, 3 - receiver, 4 - motor, 5 - electronic travel controller, 6 - servo drive, 7 – battery.

object within a given range. In addition, the module can be used as a revolution counter or rotation speed sensor. In the case of cyclic motion, KY-032 is able to record the frequency of movement and the position of an object, such as a rotor. The principle of operation is based on the detection of reflected infrared radiation. For tasks involving speed measurement, contrasting stripes - white and black - are applied to the surface of the moving part. The IR rays are directed at these stripes, and when they rotate, the sensor generates pulses whose frequency is directly proportional to the speed of movement. The module consists of two photographic components: An infrared LED and a photodetector. The infrared signal is reflected from the object and is transmitted to the receiver. The module's radiation is modulated at a frequency of 38 kHz, which provides better filtering of extraneous interference and increases the accuracy of operation.

The new sensor was tested during the tuning of the PID controller, since the correct operation of the algorithm requires a reliable and stable sensor part.

Figure 7 shows a graph of the system behavior in the mode without PID control. The graph shown in Figure 8 shows the pattern of changes in both the set and actual engine speeds in the dynamics. The unevenness in the actual rotational speed - sharp drops and peaks - can be clearly seen. These instabilities are caused by fluctuations in the load on the propeller: as the air resistance increases with the propeller pitch, the speed decreases, while as it decreases, on the contrary, there is a rapid increase in speed. This behavior indicates the need for an effective stabilization mechanism.

Figure 8 shows the effect of adding proportional control on the overall system dynamics. The introduction of a P-controller with a gain of kp=3.7 made it possible to significantly reduce the amplitude of oscillations and improve the compliance of the actual speed with the specified profile. The experimental tuning confirmed that this coefficient value is optimal within the studied conditions, as it provides a balance between the system's sensitivity and its stability. The analysis of the data in the previous graph shows a significant decrease in the deviation of the actual speed from the setpoint after the introduction of the proportional component, which confirms the increase in control accuracy.

Figure 9 shows the dynamics of the system when the differential component is added. At the value of the coefficient $kd = 15$, an increase in oscillations was recorded, indicating excessive dynamic sensitivity and approaching the stability limit. The final stage of the system tuning was the introduction of the integral component of the regulator to eliminate the residual systematic error and ensure long-term control accuracy. During the experimental optimization, it was found that the value of the integration coefficient $ki = 0.017$ provides the best quality of the transient process without excessive overshoot. The full response of the system when implementing PID control is shown in Figure 10, where the achievement of consistency between actual and reference speeds is visible. The graph in the figure shows the efficiency of the PID controller. The amplitude of sharp fluctuations in the actual rotational speed
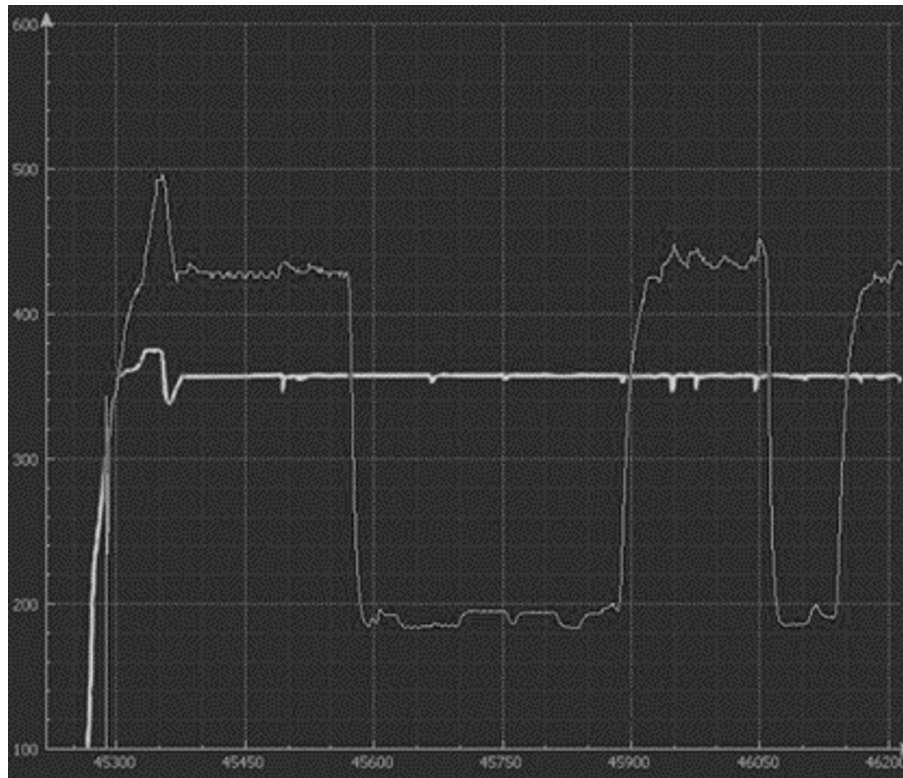
**Figure 7:** Graph of system behavior without PID controller.

caused by changes in the load on the screw has significantly decreased compared to the unregulated mode. Thanks to the integration of the PID algorithm, the system quickly returns to a stable mode after external disturbances.

During the tuning, the optimal values of the coefficients were determined: $kp = 3.7, ki = 0.017, kd = 15$. The use of these parameters provides smoother transitions when changing the angle of attack of the propeller, which indicates an increase in the quality of control and an increase in the dynamic stability of the control object.

## 4. Conclusions

The study carried out a comprehensive analysis of the principles of constructing an automated system for stabilizing the rotational speed of a variable pitch propeller. To implement the control functionality, a program module for the Arduino controller was created, which acts as a PID controller. An experimental setup has also been developed to verify the algorithm and demonstrate its performance in conditions close to real-world operating conditions.

The process of parametric tuning of the controller was based on the analysis of the transient characteristics of the system in response to external disturbances. The parameters of the PID controller were optimized by the empirical method, taking into account the nature of the oscillations and the time of the output signal establishment.

The results of the tests indicate the high efficiency of the developed algorithm: it ensures stable retention of the set value of the internal combustion engine speed equipped with a variable pitch mechanism. The results obtained are of practical importance for the design of advanced models of multicopters with internal combustion engines, which are currently at the stage of experimental implementation in the field of unmanned aerial technologies.
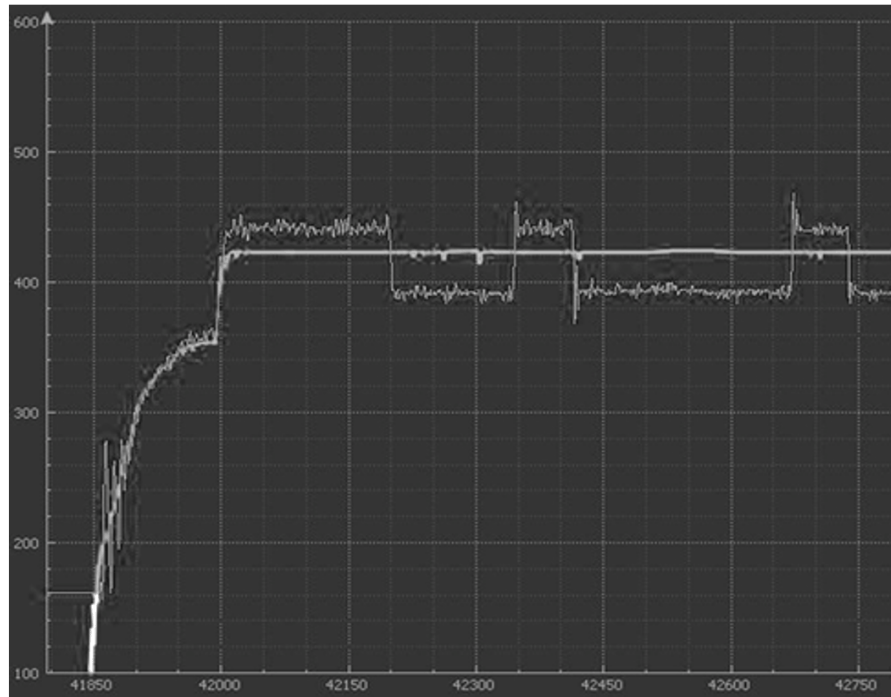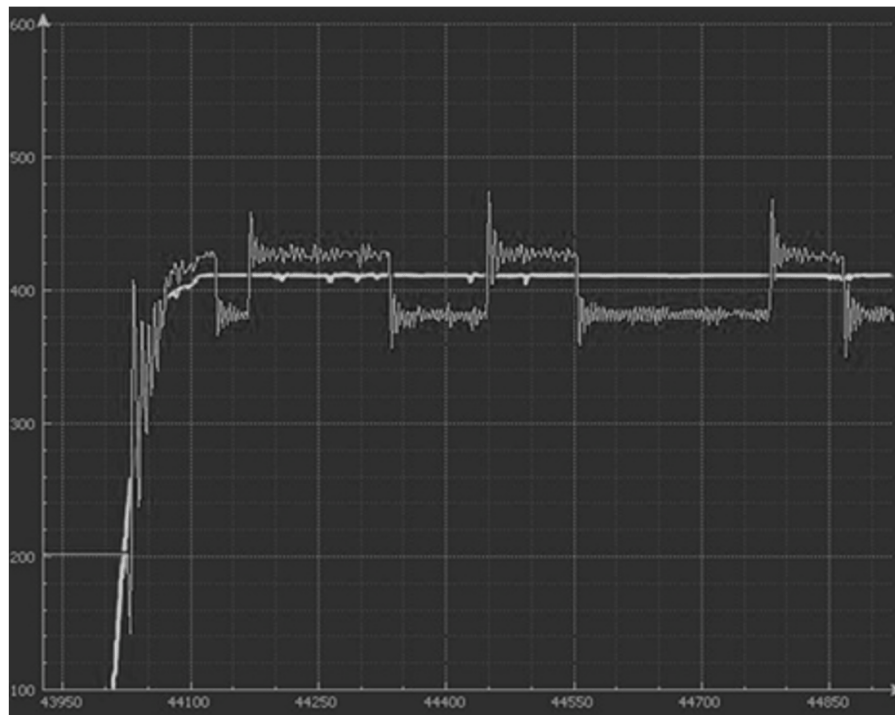
**Figure 8:** Effect of adding proportional control on the overall system dynamics
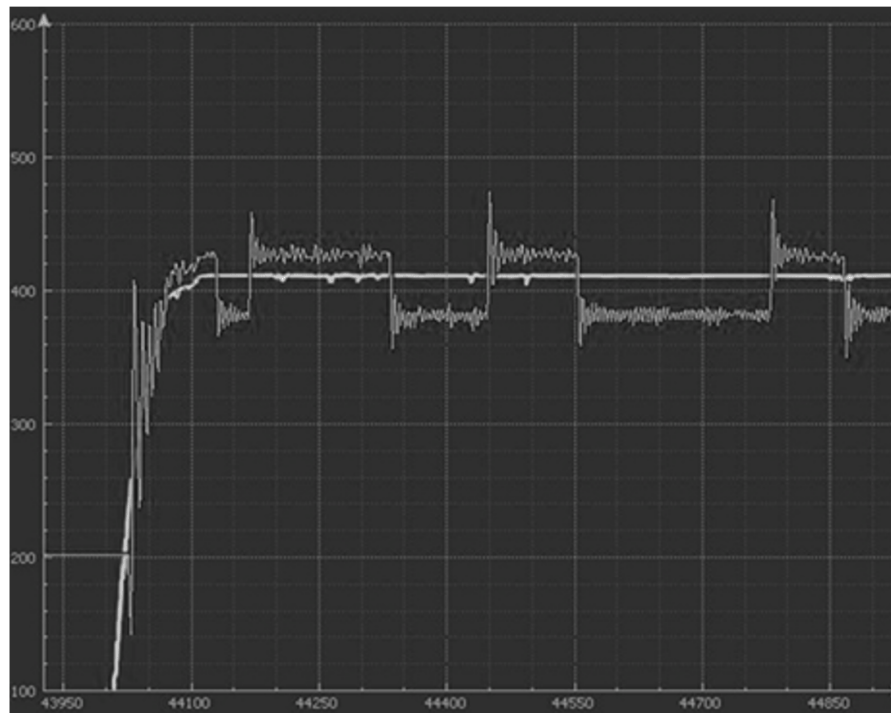


**Figure 9:** Result of PID-regulator operation.

## Declaration on Generative AI

The author(s) have not employed any Generative AI tools.

**Figure 10:** Full response of the system when implementing PID control.

# References

[1] A. Pogudin, O. Pogudina, A. Bykov, T. Plastun, Simulation of the automatic flight of a small unmanned aerial vehicle over a marker line, Open Information and Computer Integrated Technologies 0 (2022) 71–82. URL: http://nti.khai.edu/ojs/index.php/oikit/article/view/1835. doi:10.32620/oikit.2022.95.06.

[2] D. Kritskiy, S. Yashin, S. Koba, Unmanned aerial vehicle mass model peculiarities, in: S. Shkarlet, A. Morozov, A. Palagin (Eds.), Mathematical Modeling and Simulation of Systems (MODS'2020), Springer International Publishing, Cham, 2021, pp. 299–308.

[3] M. Xie, S. Xu, C. yue Su, Z. yong Feng, Y. Chen, Z. Shi, J. Lian, An adaptive recursive sliding mode attitude control for tiltrotor uav in flight mode transition based on super-twisting extended state observer, 2021. URL: https://arxiv.org/abs/2111.02046. arXiv:2111.02046.

[4] Y. N. Saravanakumar, M. T. H. Sultan, F. S. Shahar, W. Giernacki, A. Łukaszewicz, M. Nowakowski, A. Holovatyy, S. Stępień, Power sources for unmanned aerial vehicles: A state-of-the art, Applied Sciences 13 (2023). URL: https://www.mdpi.com/2076-3417/13/21/11932. doi:10.3390/app132111932.

[5] C. Amici, F. Ceresoli, M. Pasetti, M. Saponi, M. Tiboni, S. Zanoni, Review of propulsion system design strategies for unmanned aerial vehicles, Applied Sciences 11 (2021). URL: https://www.mdpi.com/2076-3417/11/11/5209. doi:10.3390/app11115209.

[6] M. Mousaei, J. Geng, A. Keipour, D. Bai, S. Scherer, Design, modeling and control for a tilt-rotor vtol uav in the presence of actuator failure, in: 2022 IEEE/RSJ International Conference on Intelligent Robots and Systems (IROS), IEEE, 2022. URL: http://dx.doi.org/10.1109/IROS47612.2022.9981806. doi:10.1109/iros47612.2022.9981806.

[7] M. Pyvovar, O. Pohudina, A. Pohudin, O. Kritskaya, Simulation of flight control of two uavs based on the "master-slave" model, in: M. Nechyporuk, V. Pavlikov, D. Kritskiy (Eds.), Integrated Computer Technologies in Mechanical Engineering - 2021, Springer International Publishing, Cham, 2022, pp. 902–907.

[8] M. Nakonechnyi, O. Ivakhiv, Y. Hirniak, Y. Nakonechnyi, O. Viter, Study of the car speed control

system using the variable structure principle, in: 2023 13th International Conference on Advanced Computer Information Technologies (ACIT), 2023, pp. 159–164. doi:`10.1109/ACIT58437.2023.10275607`.

[9] I. Lopez-Sanchez, J. Moreno-Valenzuela, Pid control of quadrotor uavs: A survey, Annual Reviews in Control 56 (2023) 100900. URL: https://www.sciencedirect.com/science/article/pii/S1367578823000640. doi:`https://doi.org/10.1016/j.arcontrol.2023.100900`.

[10] G. Ferrari, A. Onorati, G. D'Errico, Internal Combustion Engines, Società Editrice Esculapio, 2022. URL: https://books.google.com.ua/books?id=XCd9EAAAQBAJ.

[11] V. Gorantla, M. Raju, H. Shukla, Design of pi controller for level-3 electric vehicle charging station using pso, in: 2023 IEEE Renewable Energy and Sustainable E-Mobility Conference (RESEM), 2023, pp. 1–6. doi:`10.1109/RESEM57584.2023.10236295`.

[12] D. Morar, V. Mihaly, M. Şuşcă, P. Dobra, Cascade control for two-axis position mechatronic systems, Fractal and Fractional 7 (2023). URL: https://www.mdpi.com/2504-3110/7/2/122. doi:`10.3390/fractalfract7020122`.

[13] P. Bhandari, P. Z. Csurcsia, Digital implementation of the pid controller, Software Impacts 13 (2022) 100306. URL: https://www.sciencedirect.com/science/article/pii/S2665963822000458. doi:`https://doi.org/10.1016/j.simpa.2022.100306`.

[14] C. Voloşencu, Introductory chapter: Basic considerations for the digital implementation of pi controllers, in: C. Voloşencu (Ed.), PID Control, IntechOpen, Rijeka, 2025. URL: https://doi.org/10.5772/intechopen.1006482. doi:`10.5772/intechopen.1006482`.

[15] H. Al-Baidhani, M. K. Kazimierczuk, Design and implementation of digital pid control for mass-damper rectilinear systems, Mathematics 12 (2024). URL: https://www.mdpi.com/2227-7390/12/18/2921. doi:`10.3390/math12182921`.

[16] F. T. Lima, V. M. Souza, A large comparison of normalization methods on time series, Big Data Research 34 (2023) 100407. URL: https://www.sciencedirect.com/science/article/pii/S2214579623000400. doi:`https://doi.org/10.1016/j.bdr.2023.100407`.

[17] B. Pavithra, P. S. S. Rao, A. Sharmila, S. Raja, S. Sushma, Characteristics of different sensors used for distance measurement, International Research Journal of Engineering and Technology (IRJET) 4 (2017) 698–702.

[18] D. Hrubý, L. Vacho, Kubík, L. Tóth, J. Baláži, P. Kósa, M. Kišev, Characteristics of distance errors of infrared sensor relation to colour surfaces, Acta Technologica Agriculturae 25 (2022) 40–46. URL: https://doi.org/10.2478/ata-2022-0007. doi:`10.2478/ata-2022-0007`.